Chapter 6

OPTICAL PROPERTIES OF $Ho_2Ge_xTi_{2-x}O_7$ SYSTEM

6.1 Introduction

In $Ho_2Ti_2O_7$, the octahedral habit reflects the cubic symmetry of the pyrochlore structure. The amber color and strong reflectivity are indicative of band gap near the visible/ultraviolet boundary (3.2 eV). This suggests that besides exhibiting rich exotic magnetic properties, such systems could be exploited for its optical properties [98]–[100]. Several of the unusual spectroscopic properties of these pyrochlore oxides are associated with the large crystalline field that splits the electronic states of the $4f^n$ configuration of the rare earth ions [16]. A comparative study of the crystal electric field, acting on the 4f electron site based on lattice-sum calculations, was developed by Morrison [101], [102]. The inter-configurational mixing of electronic states results in different magnitude and distribution of transition intensities within the $4f^n$ electronic configuration through the substitution of non-magnetic atom at rare earth site or by varying the rare earth ion (Pr^{3+}, Eu^{3+}, $Yb^{3+,}$ etc.) itself [103]. Transition metal oxides continue to be of particular interest, due to complexities associated with d-shell electrons [104]. The 3d elements form a number of oxygen-containing clusters and compounds with variable oxidation states of the metal cation. The coloring mechanism (emission spectra) of these pyrochlore oxides and their effect on chemical pressure has not been fully investigated yet. A thorough characterization of the optical properties of these pyrochlore oxides is still lacking. We adopted a systematic approach for analyzing the crystal field states by studying the absorption and photoluminescence spectrum of these pyrochlore

oxides. The objective of this work was to induce structural distortion and to study the different multiplets of $Ho_2Ge_xTi_{2-x}O_7$ series in visible and infrared region using UV-Visible (UV-Vis; 220-1400 nm) and photoluminescence (PL) spectroscopic techniques. The spectroscopic studies of $Ho_2Ti_2O_7$ and $Ho_2Ge_2O_7$ with subsequent application of chemical pressure in its matrix has been taken up.

The aim of this chapter is to establish a correlation between the structural and optical properties of these pyrochlore oxides. The chapter is organized as follows: In the first section, we will give a brief description of already reported results of optical studies in the framework of pyrochlores, and in the second section, we will be discussing our essential findings that reveals the crystal field states identified through the optical measurements along with the determination of band-gap through Tauc plot using UV-Vis absorption spectrum.

6.2 Optical studies on $Ho_2Ti_2O_7$ system

L. Macalik et al. reported that in $Ho_2Ti_2O_7$ the transition for luminescence spectra corresponding to $^5F_5$ to $^5I_8$ electronic state involves specific vibrational levels as shown in **Figure 6.1**. The emission intensity for these vibrational transitions corresponding to given electronic levels is temperature dependent varying from 295 K to 8 K. This chapter presents the chemical pressure dependence emission intensity corresponding to these electronic levels at room temperature. This section presents the study of the optical properties of $Ho_2Ge_xTi_{2-x}O_7$ system through ultraviolet-visible spectroscopy and photoluminescence spectroscopy. The same has been discussed in section 6.2.1 and 6.2.2 respectively.

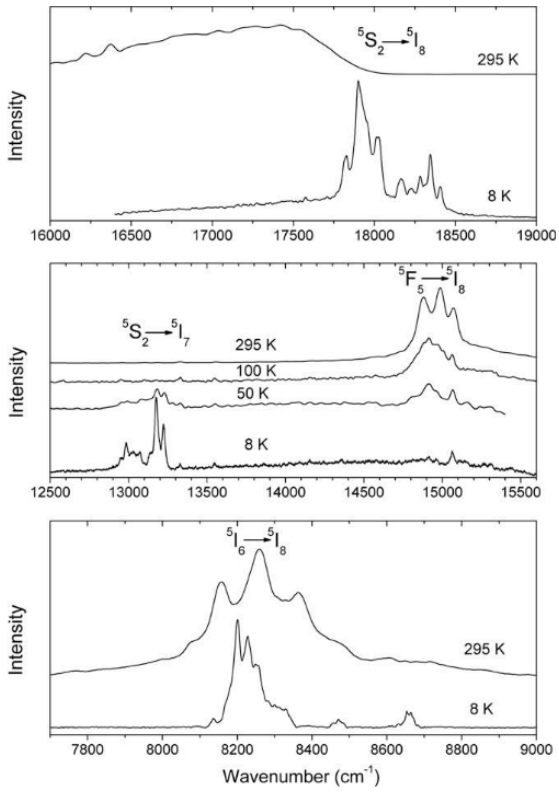

Figure 6.1 Luminescence spectra of $Ho_2Ti_2O_7$ single crystal after excitation at 488 nm (top and middle) and 1064 nm (bottom). [51]

6.2.1 Ultraviolet-visible spectroscopy

The initial determination of crystal field levels of the $Ho_2Ge_xTi_{2-x}O_7$ series had been attempted through UV-Vis absorption spectra in the wavelength range of 220-1400 nm. Numerous absorption lines as well as bands varying from low to high energy region was obtained. The absorption lines pertaining to the higher wavelength regime corresponds to low energy states of Ho^{3+} ion and has been identified as the internal transition within the 4f states. These occur as forbidden transitions within the 4f shells of the Ho^{3+} ion due to charge transfer transitions (CTT). The higher energy states in such systems are formed by the combined action of Coulomb potential of the [Xe] core of Ho^{3+}, Coulomb interaction of unpaired 4f electrons,

spin-orbit coupling and crystal field potential. These higher energy absorption peaks are due to the ligand to metal charge transfer (LMCT). Room temperature absorption spectra for $Ho_2Ge_xTi_{2-x}O_7$ are shown in **Figure 6.2.**

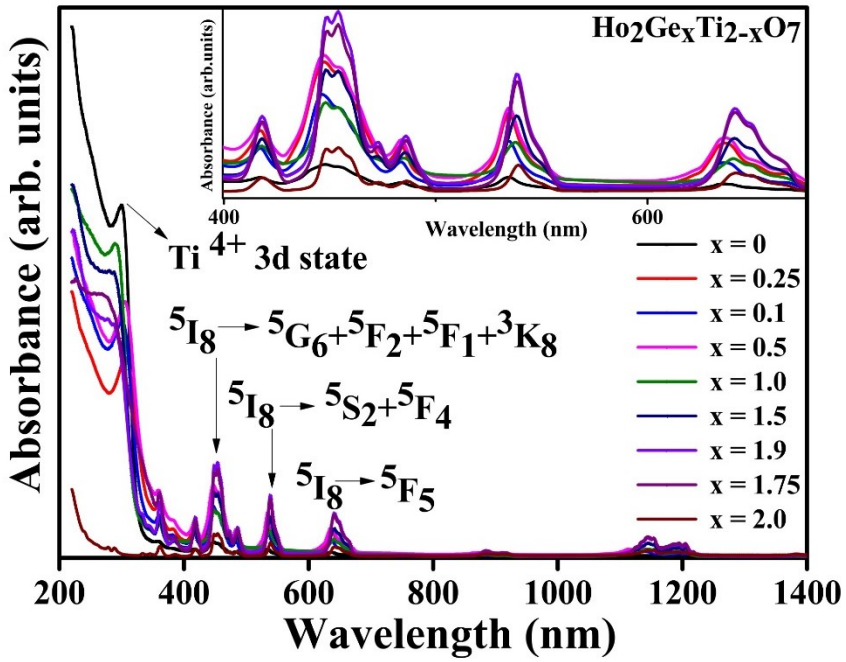

Figure 6.2 Dependence of composition on room temperature UV-Visible absorption spectra of $Ho_2Ge_xTi_{2-x}O_7$ (x=2, 1.9, 1.75, 1.5, 1, 0.5, 0.25, 0.1, 0) sample series. Inset shows the clear intensity variation in the Ho^{3+} absorption states with B site Ge^{4+} and Ti^{4+} substitution.

For x=2 i.e., in $Ho_2Ge_2O_7$ there exists a prevalent absorption peak at 240 nm equivalent to the band energy of 5.24 eV corresponding to Ge state in the conduction band (C.B.). The symmetry points and phonons involved in this transition had been shown in the chapter 5. This particular absorption between C.B. and valence band (V.B.) corresponds to an indirect electronic transition from Γ to X symmetry point involving Δ phonon. Various less intense absorption bands for Ge absorption state are also manifested in $Ho_2Ge_2O_7$ (LMCT) at 278,

288, and 333 nm involving Z to Z (direct transition), Γ to A (through indirect transition via Z and R points involving ∧, U and T phonons) and Γ to Γ (direct transition) symmetry points respectively. The symmetry points involved in these transitions are identified on the basis of making correspondence between theoretical (band structure calculation as explained in previous chapter) and experimental data. The experimental band gap is calculated applying the Tauc equation to the UV-Visible spectral data. The K points are identified from the band structure obtained from DFT calculations whose details were discussed in the previous chapter. We further applied a chemical pressure in the $Ho_2Ge_2O_7$ matrix for its effect on the electronic state and to check out the favored absorption state. With immediate Ti substitution (x=1.9) at Ge site i.e., for $Ho_2Ti_{0.1}Ge_{1.9}O_7$, the intensity of the above-mentioned transitions decreases drastically due to the appearance of immediate Ti-3d absorption band at 300 nm. This well-defined absorption state is manifested in all Ti substituted $Ho_2Ge_2O_7$ composition. The decrease in intensity of Ge absorption states and the appearance of intense Ti-3d state indicates that Ti-3d and O-2p orbital's overlapping affinity is more intense relative to O-2p and Ge-4d orbitals as explained in the chapter 5. This possible high overlapping is due to the $3d^0$ (no electron) electronic configuration of Ti state compared to Ge fully-filled $3d^{10}$ orbital in $Ho_2Ge_2O_7$, which reduces the electron-electron repulsion for $Ho_2Ti_2O_7$. It is a more preferred absorption state in $Ho_2Ge_xTi_{2-x}O_7$ since this Ti-3d state is having both a lower band-gap as well as a higher cross-section (as obtained from the DOS calculations). Not all peaks obtained from the theoretical calculations (band structure) are observed experimentally (UV-Visible spectrum) because of low transition probabilities, but all the direct transitions had been identified. UV -Vis absorbance data was employed for the experimental determination of band-gap applying Wood and Tauc equation as follows:

$$(\alpha h\nu) = A\,(h\nu - E_g)^n \qquad (6.1)$$

where α is absorption coefficient, hν is photon energy, A is a constant related to the materials, and the value of n tells the nature of the transition (n = 2, 3/2, 1/2 corresponds to the direct, direct forbidden and indirect allowed band gap respectively) [105]. Band-gap was calculated for the allowed indirect transition by noting the intercept value on the photon energy axis extrapolated up to 0 eV in a linear fit of $(\alpha h\nu)^2$ vs. hν. The obtained band gap values had been shown in the **Table 6.1**, and pictorially comparison of obtained band-gap both through theoretical and experimental approach had been represented in **Figure 6.3**, which gives clear evidence of the formation of Ti-3d state at 300 nm.

Table 6.1. Band gap energies of $Ho_2Ge_xTi_{2-x}O_7$ (x = 2, 1.9, 1.75, 1.5, 1, 0.5, 0.25, 0.1 and 0) obtained from both experimental (through Tauc plot using UV-Visible absorption spectra data) and theoretical data (DFT calculations).

Compound	Band gap (eV); experimental	Band gap (eV); theoretical
$Ho_2Ge_2O_7$	5.249	6.11
$Ho_2Ge_{1.9}Ti_{0.1}O_7$	3.920	5.89 (estimated)
$Ho_2Ge_{1.75}Ti_{0.25}O_7$	3.900	5.52
$Ho_2Ge_{1.5}Ti_{0.5}O_7$	3.897	5.39
$Ho_2Ge_1Ti_1O_7$	3.887	5.06
$Ho_2Ge_{0.5}Ti_{1.5}O_7$	3.782	4.91
$Ho_2Ge_{0.25}Ti_{1.75}O_7$	3.762	4.85
$Ho_2Ge_{0.1}Ti_{1.9}O_7$	3.759	4.34 (estimated)
$Ho_2Ti_2O_7$	3.744	4.02

Since it could be seen that the optical band gap value of 5.24 eV (Ge-4d state) in $Ho_2Ge_2O_7$ reduces drastically to 3.920 eV in $Ho_2Ge_{1.9}Ti_{0.1}O_7$ and the value lies in this range only for all Ti substituted $Ho_2Ge_2O_7$ with slight decrease with increase in Ti concentration till $Ho_2Ti_2O_7$. Hence this particular observation confirms the formation of a stable Ti state in the C.B., and the transition involves Γ to X point symmetry point mediated through Δ phonon.

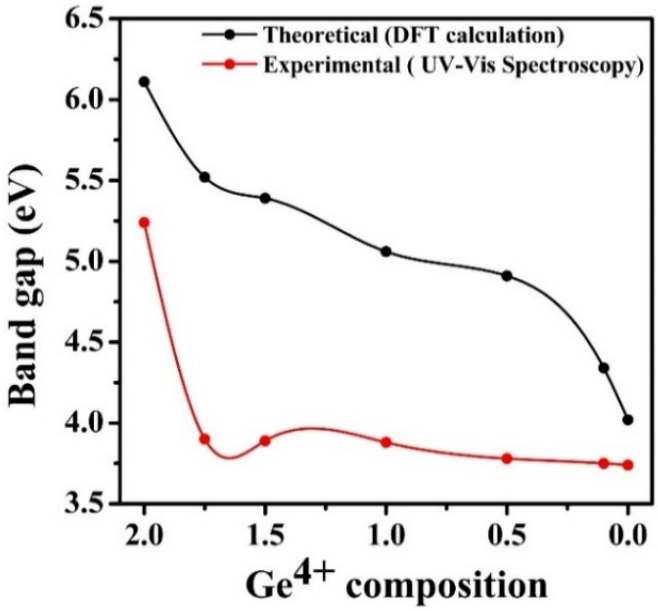

Figure 6.3 Variation in Band gap (eV) with subsequent increase in Ti^{4+} concentration in $Ho_2Ge_xTi_{2-x}O_7$.

All the other absorption bands corresponding to higher wavelength represent the Ho ion spectral line due to CTT within the 4f orbital. These 4f electrons do not take part in chemical bonding but due to the strong crystal-field effect. Its free ion ground state $^5I_8$ splits into 11 states: 6 E_g doublets, 3 A_{1g} singlet and 2 A_{2g} singlet; the excited states also split into multiple states, forming a complex pattern of absorption spectra and emission spectra [51]. These Ho^{3+} absorption lines are very intense, which theoretically verifies them to be forbidden inner shell transitions in the form of reordering within the 4f-shell. Most intense absorption band for $Ho_2Ge_xTi_{2-x}O_7$ is concentrated at 454 nm corresponding to $^5I_8$ to $^5G_6$+ ($^5F_2$ + $^5F_1$ + $^3K_8$) absorption between Ho-4f states. This is a hypersensitive transition peak that is sensitive to changes in their surroundings, and this leads to the drastic increase in the intensity of this band with chemical pressure, as could be seen from **Figure 6.2** [103].There exists symmetry

breaking at the Ho site in $Ho_2Ge_2O_7$ on Ti addition. Other absorption lines corresponding to 4f internal transitions are concentrated a 538 nm, which represents absorption from $^5I_8$ ground state to ($^5S_2$+$^5F_4$) excited state in this system. The new absorption band at 473 nm is present in $Ho_2Ge_xTi_{2-x}O_7$ till x=1.5, but it completely vanishes in $Ho_2Ti_2O_7$. The absence of this peak in $Ho_2Ti_2O_7$ indicates that it does not correspond to Ho^{3+} transition, and the origin of this absorption band is yet to be understood. Possibly this absorption may be linked with excitation to some Ge electronic state. An increase in Ti concentration in $Ho_2Ge_2O_7$ just shifts the Ho absorption bands towards the lower wavelength side coupled with peak broadening, which shows the negligible effect of lattice distortion on the splitting of the energy levels since no new absorption lines have been observed. The intensity variation is related to the change in lattice parameter. The other absorption bands within the 4f shell of Ho are centred at 360 nm, 382 nm, 418 nm, 485 nm, and 643 nm corresponding to $^5I_8$ to ($^5G_5$ + $^5H_5$), $^5I_8$ to $^5G_4$, $^5I_8$ to ($^5G_5$+$^3G_5$), $^5I_8$ to ($^5F_3$+$^3K_8$), and $^5I_8$ to $^5F_5$states [103].

6.2.2 Photoluminescence spectroscopy

In addition to absorption spectra, further we also obtained the emission spectra of the said sample series to confirm the electronic energy levels for these compositions. Since the emission spectrum depends strongly upon excitation wavelength, the same was obtained for both 290 nm and 450 nm. **Figure 6.4 (a)** and **Figure 6.4 (b)** shows the PL spectra for x = 2-1.5 & 1-0 respectively ($Ho_2Ge_xTi_{2-x}O_7$) using 290 nm excitation wavelength. For $Ho_2Ti_2O_7$, the most intense emission peak is manifested at 397 nm, which corresponds to $^5G_4$ to $^5I_8$ transition, and other emissions at 370 nm, 453 nm, 480 nm, and 522 nm are assigned to $^5G_5$ + $^3H_5$ to $^5I_8$, $^5F_2$ + $^5G_6$ + $^3K_8$ to $^5I_8$, $^5H_3$ to $^5I_8$ and $^5S_2$ to $^5I_8$ electronic transitions of Ho respectively

[106]. Immediate Ge substitution (x = 0.1) significantly increases the luminescence yield of all Ho emission peaks followed by sequential decrease with further enhanced Ge concentration for x > 0.1.

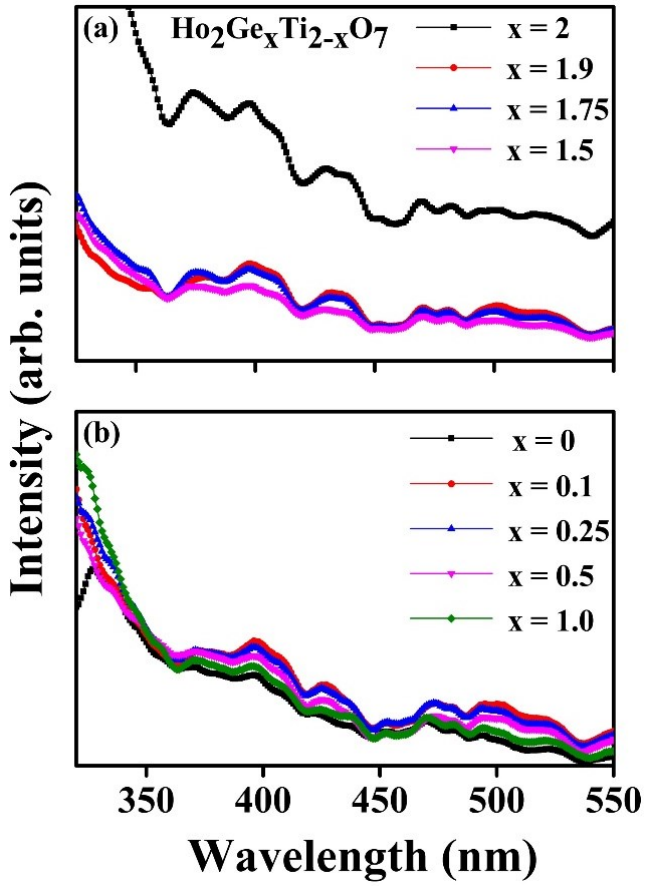

Figure 6.4 Dependence of Photoluminescence emission (PLE) spectra of (a) $Ho_2Ge_xTi_{2-x}O_7$ (x=2, 1.9, 1.75 and 1.5) (b) $Ho_2Ge_xTi_{2-x}O_7$ (x=1, 0.5, 0.25, 0.1 and 0) powdered sample series with increasing Ti^{4+} concentration in $Ho_2Ge_2O_7$ and Ge^{4+} in $Ho_2Ti_2O_7$ respectively upon excitation with 290 nm on Ho^{3+} emission states.

The emission peak identified for Ho ion obtained in $Ho_2Ti_2O_7$ is credited to two phenomena; either through ground state absorption (GSA) mechanism followed by emission within Ho-4f state or through energy transfer (ET) from excited Ti-3d state to Ho-4f states followed by

emission [106], [107]. Additional specific feature at 325 nm feature corresponds to Ti emission peak is due to ground state absorption. The transfer mechanism behind the obtained emission spectra could be explained as: In Ge substituted $Ho_2Ti_2O_7$ samples were excited using 290 nm wavelength, Ge-4d state at 333 nm gets populated due to GSA from V.B. (O-2p state), and a greater number of photons are involved in emission from Ti-3d and Ho-4f states due to ET transition from Ge-4d to Ti-3d and Ho-4f states.

However, with further increase in the concentration of Ge emission intensity corresponding to 333 nm (Ge-4d state) decreases, which indicates the enhancement of non-radiative cross-relaxation within the Ge C.B. states. Similarly, in pure $Ho_2Ge_2O_7$, emission spectra are due to GSA and direct energy transfer from Ge-4d state at 333 nm to Ho-4f excited. There exists a subsequent reduction in emission intensity for 333 nm upon Ti substitution due to ET to Ti-3d state, which appear as emission peak at 325 nm in PL spectra. The absence of this peak in $Ho_2Ge_2O_7$ emission spectra confirms it to be associated with the transition from Ti-3d state. Moreover, under the effect of crystal field d orbital splits into two sets, e_g and t_{2g} and in octahedron field, t_{2g} lies lower to e_g. There occurs ET from the Ge-4d to Ti-3d state from where electron non radiatively relaxes to the t_{2g} state from e_g by transferring energy to lattice since the d-d transition is forbidden in d^0 configuration of Ti [108]. From Ho-4f excited states, numerous Ho emission peaks are identified as down converted Stokes luminescence through non-radiative transitions within excited states and then finally transiting to $^5I_8$ ground state.

A noteworthy characteristic is manifested in PL emission spectrum using an excitation wavelength of 450 nm shown in **Figure 6.5**.

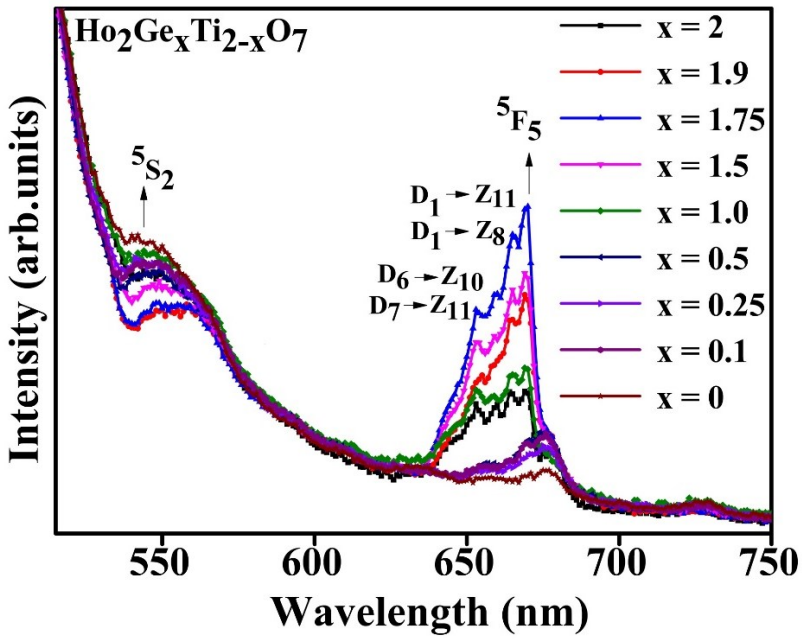

Figure 6.5 Variation in Photoluminescence Emission spectra of Ho^{3+}; $^5F_5$ to $^5I_8$ emission in $Ho_2Ge_xTi_{2-x}O_7$ (x = 2, 1.9, 1.75, 1.5 1, 0.5, 0.25, 0.1 and 0) pyrochlore oxide using excitation wavelength of 450 nm.

We were prompted to use this value of excitation wavelength since the most intense absorption band in UV-Vis spectra is concentrated at 453 nm. Hence providing a little higher excitation energy in its maximum absorbance regime might reveal some interesting results. The emission spectra exhibited three emission bands centred at 545, 666, and 727 nm and had been identified corresponding to $^5S_2$ to $^5I_8$, $^5F_5$ to $^5I_8$, and $^5S_2$ to $^5I_7$ Ho^{3+} internal 4f states transitions [106]. Ti addition in $Ho_2Ge_2O_7$ suppresses the emission peak at 545 nm with simultaneous enhancement in the emission yields at 666 nm that clearly indicates the correlation between the two adjacent states. The $^5S_2$ 4f excited state of Ho is efficiently depopulated to $^5F_5$ via relaxation process, and more favored emission corresponds from $^5F_5$ to $^5I_8$ level. $^5S_2$ is next populated from the next higher $^5F_3$ state at 483 nm; this state in turn, is

excited by absorbing 450 nm photons from $^5I_8$. An increase in Ti concentration initially increases the effective relaxation to $^5F_5$, followed by decrease in this relaxation mechanism with further increase in Ti^{4+} concentration. It is possibly related with the presence of Ho-4f emission peak at 473 nm not seen here but present in both $Ho_2Ge_2O_7$ and $Ho_2Ti_2O_7$ emission spectra (for exc. wavelength = 300 nm) and this state could be involved in relaxation mechanism.

More interesting transition is observed between $^5F_5$ and $^5I_8$ electronic levels. Systematic enhancement in emission yield is observed between certain vibrational states (Stark components) of $^5F_5$ to $^5I_8$ electronic transition, and this effect is more profound in $Ho_2Ge_2O_7$. It is due to the difference in crystal field effect at Ho site with respect to that of in $Ho_2Ti_2O_7$, which was reflected in the XPS spectra as discussed in the previous chapter. Ho ion in $Ho_2Ge_2O_7$ is located at the sites of D_{5h} symmetry and in $Ho_2Ti_2O_7$ at D_{3d} site symmetry. Because of the distortion induced in the Ho environment due to applied chemical pressure, crystal field changes, and some of the degeneracy might be removed in the sublevels of the $^5I_8$ ground states. Four favored vibronic transitions associated with $^5F_5$ (D_7, D_6, D_1, D_1) to $^5I_8$ (Z_{10}, Z_{11}, Z_8, Z_{11}) electronic levels are noticed at 652, 659, 663, and 669 nm involving D_7 to Z_{10}, D_6 to Z_{11}, D_1 to Z_8 and $D_1$to Z_{11} vibrational states [109] . All transitions are associated with the higher vibrational state of the $^5I_8$ electronic ground state. The energies involved in these transitions are shown in **Table 6.2.**

Table 6.2 Transitions associated from vibrational states of $^5F_5$ (D_7, D_6, D_1, D_1) to $^5I_8$ (Z_{10}, Z_{11}, Z_8, Z_{11}) of Ho^{3+} obtained at 652, 659, 663 and 669 nm in PLE (Photoluminescence emission) spectra with excitation wavelength of 450 nm.

Electronic state	**Vibrational state (cm^{-1})**										
$^5F_5$(Ref. 42)	D1	D2	D3	D4	D5	D6	D7				
	15558	15651	15708	15757	15785	15830	15892				
$^5I_8$ (Ref. 42)	Z1	Z2	Z3	Z4	Z5	Z6	Z7	Z8	Z9	Z10	Z11
	0	104	115	176	225	297	437	453	540	568	632
$^5F_5$ to $^5I_8$ (Transitions as observed in PL Spectra)	15892 – 568=15324		15830 – 632 = 15198			15558 – 453 =15105			15558 – 632 = 14926		
	~ 15337		~ 15174			=15105			~14947		
	= 652 nm		= 659 nm			= 662 nm			= 669nm		
	$D_7 \rightarrow Z_{10}$		$D_6 \rightarrow Z_{11}$			$D_1 \rightarrow Z_8$			$D_1 \rightarrow Z_{11}$		

The possible mechanism involved within the 4f states of the Ho^{+3} energy level diagram along with Ge^{4+} and Ti^{4+} state, as discussed above, is schematically shown in **Figure 6.6**. The absorption, as well as the emission corresponding to both 290 and 450 nm excitation wavelengths, is shown along with luminescence between specific Stark's components. The photon with 290 nm wavelength populates Ti-3d e_g state in $Ho_2Ti_2O_7$ through GSA. Ho-4f excited states get further populated by both ET from Ti-3d states and GSA. Whereas in $Ho_2Ge_2O_7$, emission peaks are due to direct energy transfer from Ge-4d state to Ho-4f excited states and ground state absorption. This notable intensity variation is coupled with the favorable vibronic transition in the visible region based on structural distortion. Such fine control over the emission spectra can find application in devices where precise wavelengths are required [107].

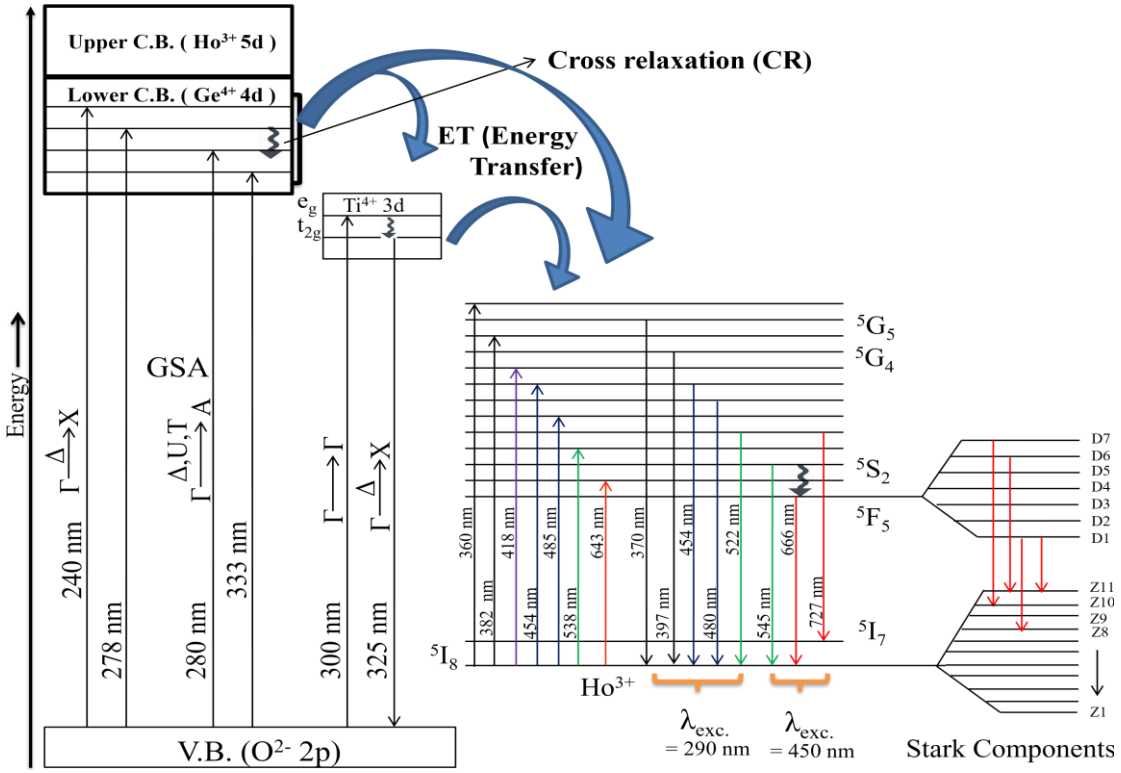

Figure 6.6 Schematic energy level scheme of Ho^{3+}, Ti^{4+} and Ge^{4+} excited states and involved emission mechanism in $Ho_2Ge_xTi_{2-x}O_7$ (x = 2, 1.9, 1.75, 1.5 1, 0.5, 0.25, 0.1 and 0) for both excitation wavelengths of 290 nm and 450 nm.

6.3 Conclusions

In $Ho_2Ge_xTi_{2-x}O_7$ pyrochlores spin ices the effect of the lattice distortion due to modification in chemical pressure alters the crystal field levels of Ho in these $Ho_2Ge_xTi_{2-x}O_7$ compounds. Band gap obtained for $Ho_2Ge_2O_7$ is 5.24 eV and gets drastically decreases to 3.92 eV (x=0.1) due to the presence of stable Ti-3d state. With a continuous increase in the Ti concentration, the band-gap further decreases to 3.74 eV for x=0. Favored sub-level transition (Specific Stark component) corresponding to $^5F_5$ to $^5I_8$ electronic transition for Ho^{3+} at $\lambda_{exc.}$ = 450 nm was

observed. Four vibronic transitions associated with $^5F_5$ (D_7, D_6, D_1, D_1) to $^5I_8$ (Z_{10}, Z_{11}, Z_8, Z_{11}) are noticed at 652, 659, 663, and 669 nm involving transitions between D_7 to Z_{10}, D_6 to Z_{11}, D_1 to Z_8, and D_1 to Z_{11} states. This subsequent insulator-semiconductor transition tenability can be explored in sensing applications [4]. These wide band-gap semiconductors tuning of electronic properties between conventional semiconductors and insulators and can be further exploited in various material applications in devices, where precise wavelengths are required.